Soot Particle Agglomeration Inlet (SPAI) for Enabling Online Chemical Composition Measurement of Nanoparticles with the Aerosol Mass Spectrometer

Sampsa Martikainen[1*], Sanna Saarikoski[2], Paxton Juuti[1], Hilkka Timonen[2], Jorma Keskinen[1], Panu Karjalainen[1]

[1] Aerosol Physics Laboratory, Tampere University, Tampere, Finland

[2]Atmospheric Composition Research, Finnish Meteorological Institute, Helsinki, Finland

Abstract

Nanoparticles are a subject of interest because of the effects they have on human health and climate. Chemical composition is one of the key properties that govern the mechanisms of these effects. However, current options for its measurement are very limited and they often require long collection times. The Soot Particle Aerosol Mass Spectrometer (SP-AMS) is an instrument designed for measuring the chemical composition of particles online. Due to losses in the sampling section of the instrument it has a lower particle size limit of 50 nm, preventing the analysis of nanoparticles. In this paper we present a measurement concept and a prototype system enabling the measurement of chemical composition of nanoparticles online. The studied nanoparticles are attached on the surfaces of artificially generated soot particles. We call this soot particle generation and agglomeration process Soot Particle Agglomeration Inlet (SPAI), which is designed as an inlet to the SP-AMS. We applied the prototype in laboratory tests, where the soot particle generation and the agglomeration section were characterized and optimized, and the performance of the SPAI was evaluated with silver nanoparticles as test aerosol. Applying the SPAI resulted in a 35-fold enhancement in the silver nanoparticle detection, compared to the measurement without it. The results indicate that the SPAI is a potential tool in resolving problems related to chemical composition measurement of nanoparticles, either as a standalone addition to the SP-AMS or combined with other sample pretreatment systems.

Keywords: Aerosol Characterization; Nanoparticle; Chemical Composition

*Corresponding author. Tel: +358503605112;

E-mail address: sampsa.martikainen@tuni.fi

INTRODUCTION

High concentrations of nanoparticles (<50 nm) are found in the atmosphere. In urban areas, they originate especially from anthropogenic sources such as traffic and small-scale combustion. Nanoparticles can have direct effects on human health and climate: the smallest nanoparticles have a high deposition efficiency in the respiratory system, and they can also translocate to other parts of the body, such as the brain (Oberdörster et al. 2004; Maher et al. 2016). Atmospheric aerosols affect the Earth's radiative forcing budget and thus climate in multiple different ways: directly through absorption/scattering of radiation and indirectly through impacts on cloud properties (Forster et al. 2007). Many of these properties are affected by the chemical composition of the particles.

The chemical composition of aerosol particles is typically studied with offline methods, by collecting material on a filter or on an impactor plate and analyzing the Particle Mass (PM) collected. Lately, online methods have become more common. An example is the Soot Particle Aerosol Mass Spectrometer (SP-AMS, Aerodyne Research Inc.), that can be used both for non-refractory substances that evaporate at the tungsten vaporizer operated at 600 ˚C, as well as for absorbing refractory components at about 4000 ˚C. The latter is made possible by the Soot Particle

(SP) module developed as an addition to the original AMS system (Onasch et al. 2012) and is typically used to quantify the amount of the refractory Black Carbon (rBC) in the aerosol.

Due to particle losses in the aerodynamic lens system in the inlet of the SP-AMS, the transmission efficiency of particles smaller than 50 nm or larger than 1 µm (vacuum aerodynamic diameter) is poor (Liu et al. 2007), meaning that a major fraction of nanoparticles is left out of reach. With the SP-module also comes a challenge of overlapping the particle and laser beams: the collection efficiencies of both rBC and the particle matter associated with it are strongly influenced by the overlap. The overlap in turn is affected by particle properties, as the divergence from the center of the particle beam depends on the particle size, morphology and chemical composition. (Liu et al. 1995; Huffman et al. 2005; Willis et al. 2014) Particles that neither absorb the wavelength of the laser (1064 nm) nor evaporate at 600 ˚C cannot be detected by the instrument.

The options for measuring the chemical composition of nanoparticles online are very limited. Combining a Scanning Mobility Particle Sizer (SMPS) and an Inductively Coupled Plasma Mass Spectrometer (ICP-MS) has been presented (Hess et al. 2015). The drawbacks of this system are high cost and low portability. Single Particle Mass Spectrometry (SPMS) can be used to analyze the chemical composition and size of single particles in near real-time. Examples of such instruments are Aerosol Time-of-Flight Mass Spectrometer (ATOFMS, Prather et al. 1994) and Single Particle Laser Ablation Time-of-Flight Mass Spectrometer (SPLAT-MS, Zelenyuk and Imre

2005). These techniques suffer from particle losses before the detection part of the instrument as well, and they are limited by their nonquantitative nature. There is a fundamental need for a system that could be applied in all sorts of measurement environments to study the detailed nanoparticle composition online.

In this study we present a measurement concept and a prototype system enabling the measurement of chemical composition of nanoparticles online. In the concept, the studied nanoparticles are attached on the surfaces of artificially generated soot particles. We call this soot particle generation and agglomeration process the Soot Particle Agglomeration Inlet (SPAI). The system is designed as an inlet to the SP-AMS. We applied the prototype in laboratory tests, where the soot particle generation and the agglomeration section were characterized and optimized, and the performance of the SPAI was evaluated with silver nanoparticles as test aerosol.

THE CONCEPT OF THE SPAI

The concept of the SPAI is illustrated in Fig 1. The unknown aerosol is mixed with soot particles and led to an agglomeration chamber, a large volume compared to the sample line, resulting in a long residence time. The studied particles then coagulate with the soot particles. The sample flow is created with an Ejector Diluter (ED), after which the mixture is led to the SP-AMS. The desired

test- and soot aerosol flows are set by constricting the lines with adjustable valves. In the protype system, the soot particles are generated by burning acetylene (C_2H_2) with a Flat Flame Burner (McKenna Inc.) under fuel-rich conditions, but any device capable of producing a suitable soot mode is a viable option. The combustion products are treated with a Catalytic Stripper (CS, Amanatidis et al. 2018) operating at 350 ˚C to remove volatile compounds, ideally leaving only the non-volatile fraction of soot.

Downstream the agglomeration chamber, ideally all the tested aerosol particles are attached to soot particles mainly larger than 50 nanometers in size and can thus penetrate the aerodynamic lens. Soot particles then reach the laser in the SP part, absorbing a great deal of energy. Heat is transferred from the high-temperature soot particles to the coating. Ideally, both the soot and coating are entirely evaporated, further ionized, and efficiently transferred to the detection part of the instrument.

METHODS

The test aerosol was created by producing silver particles with a tube furnace method (Scheibel and Porstendörfer 1983), using nitrogen as carrier gas. Silver particles were chosen as the test aerosol for two main reasons. Firstly, silver has properties that we were looking for in the

benchmarking tests: it is a nonvolatile metal that does not evaporate in the vaporizer and it has two distinctive isotopes in the AMS High Resolution spectrum (m/z 106.905 and 108.905). Secondly, our laboratory infrastructure for generation of silver nanoparticles is well established and we are experienced in controlling e.g. the size distributions of the particles. The SP-AMS has been shown to be sensitive to silver (and other metal) particles as is (Nilsson et al. 2015). However, the addition of SPAI provides the advantages of (1) increased penetration of nanoparticles through the aerodynamic lens and (2) more efficient evaporation of the reflective elements, as they lie on the surfaces of soot particles that absorb the wavelength of the laser extremely well.

An SMPS (TSI) operated with model 3081 Differential Mobility Analyzer (DMA) was used to determine the particle size distribution. Particle densities at selected particle diameters (17.8 nm and 112 nm) were determined with a Cambustion Centrifugal Particle Mass Analyzer (CPMA, Olfert and Collings 2005) coupled with a DMA.

Adjusting the furnace temperature allowed for manipulation of the silver particle size distribution. Similarly, the soot particle properties were varied by adjusting fuel flow and thus the stoichiometric ratio of combustion. Prior to the measurements, both generation systems were tested to determine how the adjusted parameters affect the generated particles and to find a few distinctive soot and silver particle size distributions for the tests. The stabilities of the systems with the chosen parameter values were also verified. In the tests, a cylinder-shaped volume of approximately 7 liters

126 was used as the agglomeration chamber. With the inlet flow of the ED (4.7 lpm), the residence time
127 in the agglomeration section is estimated to be 90 seconds.

128 Three different silver modes were tested, corresponding to furnace temperatures of 1100 ˚C,
129 1150 ˚C and 1200 ˚C. Similarly, three soot modes were generated, corresponding to burner fuel
130 feeds of 0.9 lpm, 0.92 lpm and 0.95 lpm. The modes are from now on referred to as "low", "med"
131 and "high", referring to both the concentration of the generated substance (silver or soot) and the
132 adjusted parameters (temperature or flow).

133 The measured silver modes extended below the lower size limit of the SMPS (6.85 nm). In order
134 to accurately estimate how much silver agglomerated with soot, modal fits for the measured size
135 distributions were constructed by assuming a lognormal size distribution

136

137 $$\frac{dN}{dln(D_p)} = \frac{N_{tot}}{\sqrt{2\pi}ln(\sigma_g)} exp\left(-\frac{(ln(D_p)-ln(D_g))^2}{2\,ln^2(\sigma_g)}\right) \quad (1)$$

138

139 where N is the particle concentration, D_P particle diameter, N_{tot} total particle concentration, σ_g
140 geometric standard deviation and D_g the geometric mean diameter. The appropriate values for these
141 variables were found by least squares method, minimizing the error between the fit and measured
142 values.

The SP-AMS is a mass-based instrument and in order to compare the concentrations measured by it and the SMPS, the number concentrations needed to be converted to mass concentrations. In order to achieve this, silver particle density as a function of particle diameter was needed. Silver particles generated with the tube furnace method form agglomerates (Scheibel and Porstendörfer 1983; Ku and Maynard 2006). Using the fractal dimension of the agglomerates, the effective density of particles can be described as

$$log(\rho_{eff}) = -(3 - fd)\, log\left(\frac{D_{mob}}{D_{ref}}\right) + log(\rho_{ref}) \quad (2)$$

where ρ_{eff} is the effective density, fd the fractal dimension, D_{mob} the mobility diameter and D_{ref} the upper diameter limit for particles with the reference density ρ_{ref} and spherical shape. The density of agglomerate-shaped particles has been successfully described with this method in previous studies (e.g. Ristimäki 2006, Skillas et al. 1998).

The effective density of silver particles was determined for two mobility diameters (17.8 nm and 112 nm, corresponding to densities of 6.11 g cm^{-3} and 2.30 g cm^{-3}, respectively). If the density of silver at room temperature (10.49 g cm^{-3}) is assumed as the reference density ρ_{ref}, the remaining unknown variables fd and d_{ref} can be solved from Equation 2, which yields 2.3035 and 6.1106 nm, respectively.

The validity of the density function was tested by the following method. First, the number size distribution of the generated silver particles was measured without the agglomeration chamber. It was then measured again after the agglomeration chamber, letting the particles grow due to agglomeration. Thus, two different size distributions with equal mass were obtained. After calculating the mass concentrations with and without the density correction and comparing the obtained results, it was found that assuming constant density resulted in almost threefold difference, whereas applying the density correction resulted in a difference less than 4%.

The particle diameters in the distributions measured with the SMPS are electrical mobility diameters, whereas the mentioned SP-AMS cutoff (~50 nm) is a vacuum aerodynamic diameter. In order to link the two, a relation presented by Jimenez et al. (2003) was used:

$$D_{va} = \frac{\rho_p D_v}{\rho_0 X_v}, \quad (3)$$

where D_{va} is the vacuum aerodynamic diameter, D_v is the volume equivalent diameter, X_v is the dynamic shape factor, ρ_p is the density of the particle material and ρ_0 is unit density. For a spherical particle $D_v = D_{mob}$ and $X_v = 1$. Thus, a spherical silver particle with a vacuum aerodynamic diameter of 50 nm has a mobility diameter of 4.8 nm. Since the upper diameter limit for spherical particles was determined to be 6.11 nm, the spherical shape assumption is valid.

The data obtained with the SP-AMS was analyzed with Igor Pro (v. 6.37) software, including packages Squirrel (v. 1.57) and Pika (v. 1.16). Collection Efficiency (CE) and Relative Ionization Efficiency (RIE) of 1 were used for the calculation of silver mass. Prior to the measurements, default calibrations with ammonium nitrate and Regal black were performed. The main goal for the measurements was to generally test the functionality of the concept and thus no specific calibration for silver was performed.

RESULTS AND DISCUSSION

Results from the laboratory tests are shown in Fig. 2. The subfigures on the right side (b and d) contain the size distributions obtained while varying the soot or silver feed while keeping the other constant. Both the measured distributions and the modal fits are shown. The red line labeled as "Transmission limit" represents the vacuum aerodynamic diameter of 50 nm, converted to electrical mobility diameter (4.8 nm) as presented in the section "Methods". In the left subfigures (a and c), the corresponding calculated elemental silver mass concentrations from the SP-AMS are shown. Note that one measurement point (high silver feed combined with low soot feed) is presented in both upper and lower subfigures. Further results obtained from the measured silver concentrations and particle size distributions are presented in Table 1.

With constant soot feed (low), varying the silver feed increases the silver mass detected by SP-AMS (0.32 µg m^{-3}, 1.44 µg m^{-3} and 5.75 µg m^{-3} for low, medium, and high silver feed, respectively), which is seen in subfigure c. The agglomerated silver does not cause a visible change in the soot mode (subfigure d).

Larger soot modes scavenge more silver particles which can be seen from the size distributions in subfigure b. The scavenged silver mass fractions are 0.80, 0.89 and 0.97 for low, medium, and high soot feeds, respectively. Changing the soot feed had a dramatic impact on the silver detected with the SP-AMS. Without soot, the measured concentration was 0.3 µg m^{-3}. With low, medium, and high soot feed the detected silver concentrations were approximately 6 µg m^{-3}, 8 µg m^{-3} and 11 µg m^{-3}, respectively. In other words, applying the SPAI increased the silver detection by a factor of up to 35. Due to high density, even small (in terms of electrical mobility diameter) silver particles are able to penetrate the aerodynamic lens. The increased silver detection in the SP-AMS is thus mainly attributed to the enhancement in the evaporation (and consequently in the RIE) of silver in the SP-AMS.

Looking at the measurement points presented in Table 1, silver mass agglomerated with soot (estimated from the size distributions as presented in the section “Methods”) is 6-10 times higher than the silver mass detected by SP-AMS. This is explained partly by the instrument not being

214 calibrated for silver and partly by silver simply not reaching the detection part of the instrument,
215 due to agglomeration with suboptimal-sized soot particles.
216
217 ## CONCLUSIONS
218
219 The initial results of the SPAI prototype testing on nanoparticle composition are promising.
220 While this method has been tested for silver nanoparticles, it can in principle be used for any type
221 of nanoparticles. However, it is most suitable for species that are not included in the generated soot
222 aerosol, e.g. metals.
223 Further research on the SPAI should focus on the calibrations of the SP-AMS system together
224 with the SPAI inlet for several substances, choosing an optimal soot particle size distribution and
225 application-specific development of the system. E.g. in the field of engine exhaust emissions, the
226 knowledge on the chemical composition of sub-23 nanometer particles is insufficient. Ideally, the
227 soot particles should have a high penetration through the aerodynamic lens, high absorptivity at
228 1064 nm wavelength (that of the laser in the SP-module), a simple background spectrum and enable
229 a high rate of agglomeration of unknown particles on soot.
230 The studied aerosol can be combined with other sample pretreatment systems in order to
231 examine the chemical composition of a certain fraction of the aerosol. The non-volatile fraction

could be investigated by using a thermal denuder, a catalytic stripper or an aerosol gas exchange system (Bainschab et al. 2019). A pre-impactor, DMA, CPMA or a differential diffusion analyzer (Arffman et al. 2017) could be used to choose particles of certain size range. An aerosol concentrator (Saarikoski et al. 2019) can improve the signal originating from nanoparticles since their mass concentration generally tends to be low.

ACKNOWLEDGMENTS

This work was conducted partly in DownToTen project, funded by the European Union's Horizon 2020 research and innovation programme under grant agreement Nr. 724085. S.M. acknowledges funding from Kone Foundation, and P.K. acknowledges funding from Academy of Finland project EFFi decision Nr. 322120.

DISCLAIMER

The authors declare that there is no conflict of interest.

REFERENCES

Amanatidis, S., Ntziachristos, L., Karjalainen, P., Saukko, E., Simonen, P., Kuittinen, N., Aakko-Saksa, P., Timonen, H., Rönkkö, T., and Keskinen, J. 2018. "Comparative Performance of a Thermal Denuder and a Catalytic Stripper in Sampling Laboratory and Marine Exhaust Aerosols." *Aerosol Sci. Technol.* 52 (4): 420–32. https://doi.org/10.1080/02786826.2017.1422236.

Arffman, A., Juuti, P., Harra, J., and Keskinen, J. 2017. "Differential Diffusion Analyzer." *Aerosol Sci. Technol.* 51 (12): 1429–37. https://doi.org/10.1080/02786826.2017.1367089.

Bainschab, M., Martikainen, S., Keskinen, J., Bergmann, A., and Karjalainen, P. 2019. "Aerosol Gas Exchange System (AGES) for Nanoparticle Sampling at Elevated Temperatures: Modeling and Experimental Characterization." *Sci. Rep.* 9 (1). https://doi.org/10.1038/s41598-019-53113-5.

Forster, P., Ramaswamy, V., Artaxo, P., Berntsen, T., Betts, R., Fahey, D.W., Haywood, J., Lean, J., Lowe, D.C., Myhre, G. et al. 2007. Changes in Atmospheric Constituents and in Radiative Forcing. *Climate Change 2007: The Physical Science Basis. Contribution of Working Group I to the Fourth Assessment Report of the Intergovernmental Panel on Climate Change [Solomon, S., D. Qin, M. Manning, Z. Chen, M. Marquis, K.B. Averyt, M.Tignor and H.L.*

267 *Miller (eds.)]*. Cambridge University Press, Cambridge, United Kingdom and New York, NY,
268 USA.
269 Hess, A., Tarik, M., and Ludwig, C. 2015. "A Hyphenated SMPS-ICPMS Coupling Setup: Size-
270 Resolved Element Specific Analysis of Airborne Nanoparticles." *J. Aerosol Sci.* 88: 109–18.
271 https://doi.org/10.1016/j.jaerosci.2015.05.016.
272 Huffman, J.A., Jayne, J.T., Drewnick, F., Aiken, A.C., Onasch, T., Worsnop, D.R., and Jimenez,
273 J.L. 2005. "Design, Modeling, Optimization, and Experimental Tests of a Particle Beam
274 Width Probe for the Aerodyne Aerosol Mass Spectrometer." *Aerosol Sci. Technol.* 39 (12):
275 1143–63. https://doi.org/10.1080/02786820500423782.
276 Jimenez, J.L., Bahreini, R., Cocker III, D.R., Zhuang, H., Varutbangkul, V., Flagan, R.C., Seinfeld,
277 J.H., O'Dowd, C.D., and Hoffmann, T. 2003. "New Particle Formation from Photooxidation
278 of Diiodomethane (CH2I2)." *J. Geophys. Res. Atmos.* 108 (D10).
279 https://doi.org/https://doi.org/10.1029/2002JD002452.
280 Ku, B.K., and Maynard, A.D. 2006. "Generation and Investigation of Airborne Silver
281 Nanoparticles with Specific Size and Morphology by Homogeneous Nucleation, Coagulation
282 and Sintering." *J. Aerosol Sci.* 37 (4): 452–70.
283 https://doi.org/https://doi.org/10.1016/j.jaerosci.2005.05.003.
284 Liu, P., Ziemann, P.J., Kittelson, D.B., and McMurry, P.H. 1995. "Generating Particle Beams of

Controlled Dimensions and Divergence: II. Experimental Evaluation of Particle Motion in Aerodynamic Lenses and Nozzle Expansions." *Aerosol Sci. Technol.* 22 (3): 314–24. https://doi.org/10.1080/02786829408959749.

Liu, P.S.K., Deng, R., Smith, K.A., Williams, L.R., Jayne, J.T., Canagaratna, M.R., Moore, K., Onasch, T.B., Worsnop, D.R., and Deshler, T. 2007. "Transmission Efficiency of an Aerodynamic Focusing Lens System: Comparison of Model Calculations and Laboratory Measurements for the Aerodyne Aerosol Mass Spectrometer." *Aerosol Sci. Technol.* 41 (8): 721–33. https://doi.org/10.1080/02786820701422278.

Maher, B.A., Ahmed, I.A.M., Karloukovski, V., MacLaren, D.A., Foulds, P.G., Allsop, D., Mann, D.M.A., Torres-Jardón, R., and Calderon-Garciduenas, L. 2016. "Magnetite Pollution Nanoparticles in the Human Brain." *Proc. Natl. Acad. Sci.* 113 (39): 10797–801. https://doi.org/10.1073/pnas.1605941113.

Nilsson, P.T., Eriksson, A.C., Ludvigsson, L., Messing, M.E., Nordin, E.Z., Gudmundsson, A., Meuller, B.O., et al. 2015. "In-Situ Characterization of Metal Nanoparticles and Their Organic Coatings Using Laser-Vaporization Aerosol Mass Spectrometry." *Nano Res.* 8 (12): 3780–95. https://doi.org/10.1007/s12274-015-0877-9.

Oberdörster, G., Sharp, Z., Atudorei, V., Elder, A., Gelein, R., Kreyling, W., and Cox, C. 2004. "Translocation of Inhaled Ultrafine Particles to the Brain." *Inhal. Toxicol.* 16 (6–7): 437–45.

https://doi.org/10.1080/08958370490439597.

Olfert, J.S., and Collings, N. 2005. “New Method for Particle Mass Classification - The Couette Centrifugal Particle Mass Analyzer.” *J. Aerosol Sci.* https://doi.org/10.1016/j.jaerosci.2005.03.006.

Onasch, T.B., Trimborn, A., Fortner, E.C., Jayne, J.T., Kok, G.L., Williams, L.R., Davidovits, P., and Worsnop, D.R. 2012. “Soot Particle Aerosol Mass Spectrometer: Development, Validation, and Initial Application.” *Aerosol Sci. Technol.* 46 (7): 804–17. https://doi.org/10.1080/02786826.2012.663948.

Prather, K.A., Nordmeyer, T., and Salt, K. 1994. “Real-Time Characterization of Individual Aerosol Particles Using Time-of-Flight Mass Spectrometry.” *Anal. Chem.* 66 (9): 1403–7. https://doi.org/10.1021/ac00081a007.

Ristimäki, J. 2006. "Sampling and Measurement Methods for Diesel Exhaust Aerosol." Doctoral dissertation. Tampere University. Retrieved from: http://urn.fi/URN:NBN:fi:tty-200810021102

Saarikoski, S., Williams, L.R., Spielman, S.R., Lewis, G.S., Eiguren-Fernandez, A., Aurela, M., Hering, S. V., et al. 2019. “Laboratory and Field Evaluation of the Aerosol Dynamics Inc. Concentrator (ADIc) for Aerosol Mass Spectrometry.” *Atmos. Meas. Tech.* 12 (7): 3907–20. https://doi.org/10.5194/amt-12-3907-2019.

321 Scheibel, H.G., and Porstendörfer, J. 1983. “Generation of Monodisperse Ag- and NaCl-Aerosols
322 with Particle Diameters between 2 and 300 Nm.” *J. Aerosol Sci.* 14 (2): 113–26.
323 https://doi.org/https://doi.org/10.1016/0021-8502(83)90035-6.
324 Skillas, G., Künzel, S., Burtscher, H., Baltensperger, U., and Siegmann, K. 1998. “High Fractal-
325 like Dimension of Diesel Soot Agglomerates.” *J. Aerosol Sci.* 29 (4): 411–19.
326 https://doi.org/10.1016/S0021-8502(97)00448-5.
327 Willis, M.D., Lee, A.K.Y., Onasch, T.B., Fortner, E.C., Williams, L.R., Lambe, A.T., Worsnop,
328 D.R., and Abbatt, J.P.D. 2014. “Collection Efficiency of the Soot-Particle Aerosol Mass
329 Spectrometer (SP-AMS) for Internally Mixed Particulate Black Carbon.” *Atmos. Meas. Tech.*
330 7 (12): 4507–16. https://doi.org/10.5194/amt-7-4507-2014.
331 Zelenyuk, A., and Imre, D. 2005. “Single Particle Laser Ablation Time-of-Flight Mass
332 Spectrometer: An Introduction to SPLAT.” *Aerosol Sci. Technol.* 39 (6): 554–68.
333 https://doi.org/10.1080/027868291009242.
334

Table 1: The effect of soot feed of SPAI on the silver agglomerated with soot (mass and number), agglomeration ratio (the fraction of silver agglomerated with soot), silver mass detected by SP-AMS, detection ratio of SP-AMS (the fraction of silver mass agglomerated with soot that is detected) and improvement in the silver detection of SP-AMS.

[1]With default SP-AMS calibration.

Soot feed	**Silver agglomerated with soot**		**Agglomeration ratio**		**Silver mass[1] (SP-AMS, µg m^{-3})**	**SP-AMS detec. ratio[1]**	**Detec. improvement factor**
	Mass (µg m^{-3})	*Number (10^6 cm^{-3})*	*Mass*	*Number*			
None	-	-	-	-	0.30	-	-
Low	54.63	1.192	0.801	0.558	5.84	0.107	19.2
Med	60.47	1.606	0.887	0.752	8.18	0.135	26.9
High	66.07	1.997	0.969	0.935	10.73	0.162	35.4

Figure Captions

Fig. 1. The concept of the SPAI.

Fig. 2. Enhancement of elemental silver detection in the SP-AMS by the level of generated soot and silver (subfigures a and c) and corresponding particle size distributions from SMPS (subfigures b and d). Red line represents the vacuum aerodynamic diameter of 50 nm converted to electrical mobility, assuming the density of silver and spherical shape of particles.

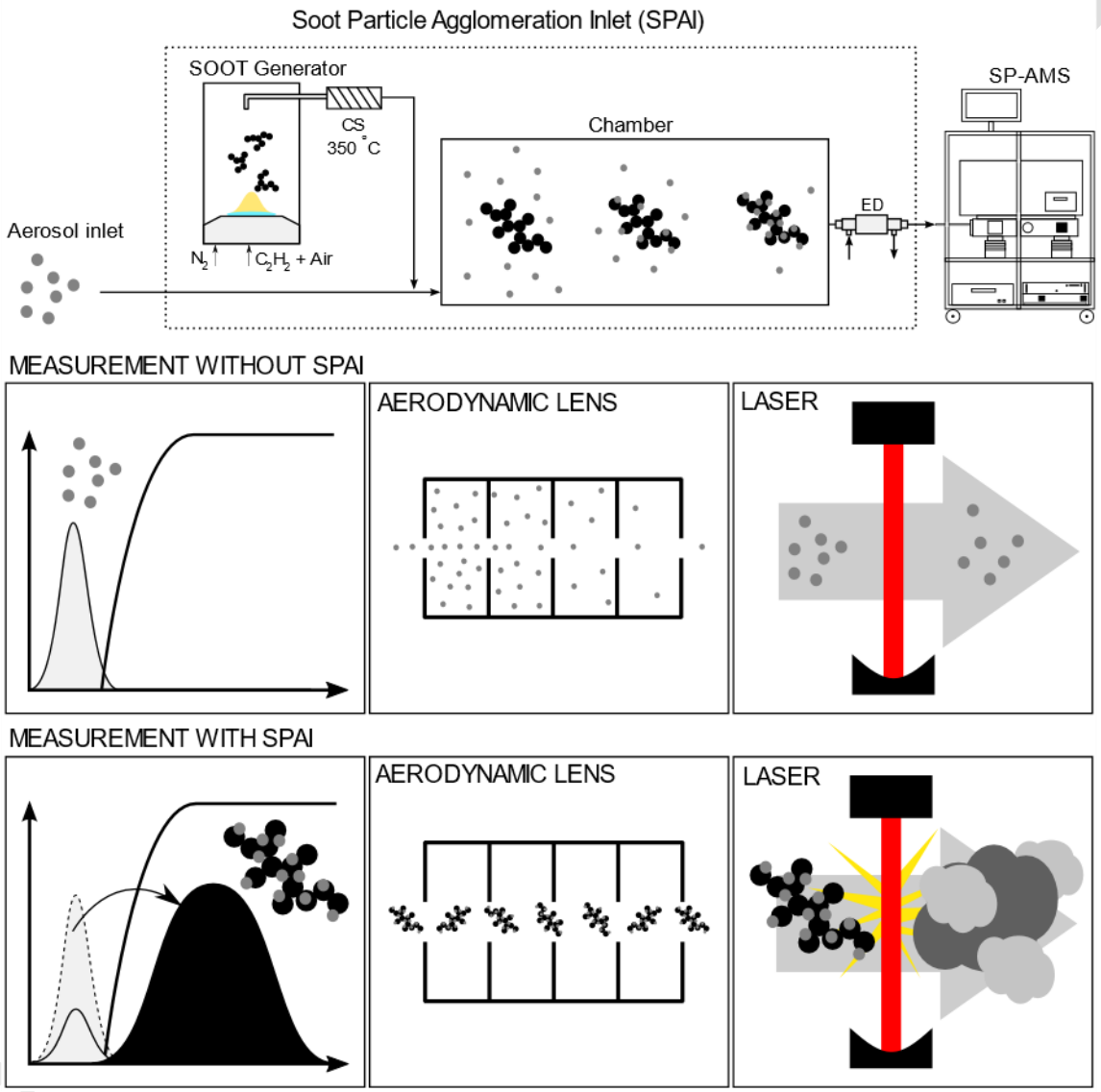
Soot Particle Agglomeration Inlet (SPAI)
SOOT Generator
CS
350 °C
Chamber
SP-AMS
ED
Aerosol inlet
N2
C2H2 + Air
MEASUREMENT WITHOUT SPAI
AERODYNAMIC LENS
LASER
MEASUREMENT WITH SPAI
AERODYNAMIC LENS
LASER

Fig. 1.

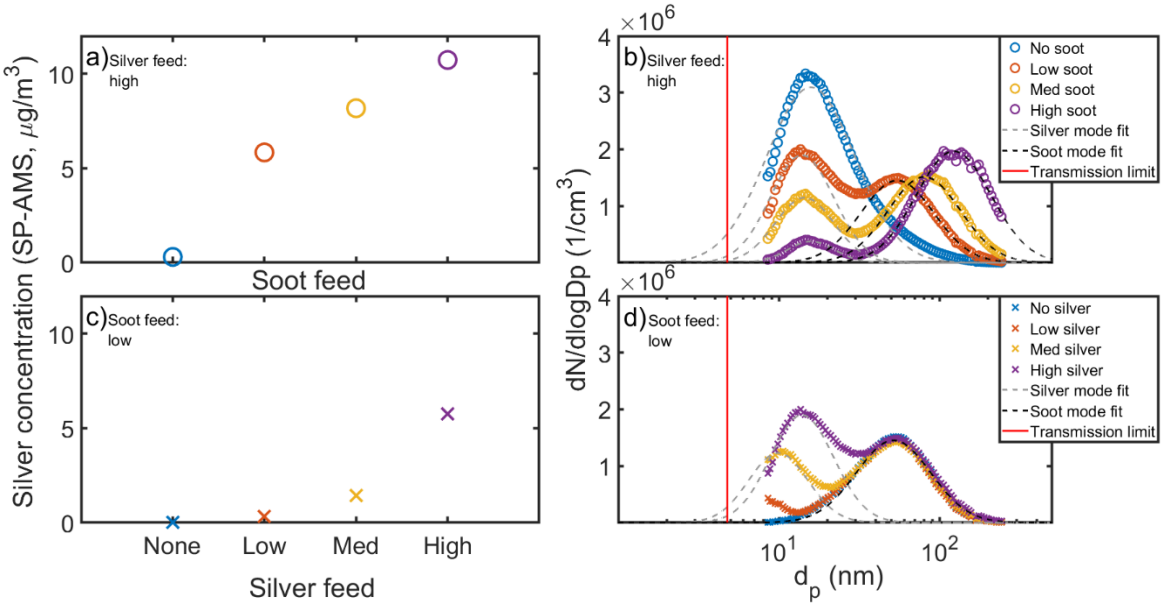

Fig. 2.